Hybrid Miniature Fabry–Perot Sensor with Dual Optical Cavities for Simultaneous Pressure and Temperature Measurements

Hyungdae Bae, David Yun, Haijun Liu, Douglas A. Olson, and Miao Yu

***Abstract*—We present a novel hybrid miniature dual-cavity Fabry–Perot sensor for simultaneous pressure and temperature measurements. The pressure sensing cavity is composed of an UV-molded cavity covered by a metal/polymer composite diaphragm for achieving a high pressure sensitivity while maintaining a miniature sensor size. Another intrinsic polymer/silica cavity is adopted for temperature sensing, which enables a high temperature sensitivity even with a short cavity length due to the large thermal expansion of the polymer. The sensor is fabricated by using a unique UV molding process with simple and safe procedures. The overall sensor size is around 150 μm in diameter and 343 μm in length. Experimental studies show that the sensor exhibits a good linearity over a pressure range of 6.89 to 27.58 kPa with a pressure sensitivity of 0.0122 μm/kPa at 26 °C, and a temperature range of 26.0 °C to 50.0 °C with a temperature sensitivity of 0.0029 μm/°C. An optical signal processing method is developed to retrieve the two cavity length changes, which is demonstrated to have a better resolution and a faster speed than the conventional method. The sensor is expected to benefit many fronts that require simultaneous pressure and temperature measurements with minimum intrusiveness, especially for biomedical applications.**

***Index Terms*—Fabry–Perot (FP), fiber optics, optical sensors, optical signal processing.**

I. Introduction

MINIATURE fiber optic Fabry–Perot (FP) sensors have attracted much interest for pressure monitoring due to their advantages of small size, high sensitivity, immunity to electromagnetic interference, and convenience of light guiding/detection through optical fibers [1]. Many different types of FP pressure sensors have been demonstrated. Most of these sensors are built with silicon/silica/ceramic materials [2]–[13] that have good mechanical, chemical, and thermal stabilities. However, due to the large elastic modulus of silica/silicon/ceramic, developing a high sensitivity miniature sensor becomes difficult. In addition, fabrication of these sensors often involves high temperature and harsh acid. On the other hand, to realize a high sensitivity, polymer materials become an attractive choice for miniature pressure sensors [14]–[16], since its Young's modulus is significantly smaller than that of silicon/silica/ceramic. Moreover, polymer processes can be performed under ambient pressure and temperature without hazardous chemicals. However, a significant drawback of a polymer-based sensor is the high temperature sensitivity, which must be compensated to obtain accurate pressure measurements.

To compensate the temperature effect, one method is to include a fiber Bragg grating (FBG) as a temperature sensor in the pressure sensor design [16]–[19]. However, since the length of the embedded FBG is usually more than several millimeters, even when the FBG is placed close to the FP cavity, the temperature measuring location from the FBG is still away from the pressure sensing cavity, making it difficult to obtain the temperature at the pressure sensing location. Furthermore, this method often requires using a spectrometer with a large wavelength range or two separate spectrometers for resolving the spectra of both the FBG and FP sensors, which makes the system more expensive. In addition, adding a FBG sensor to a pressure sensor can increase the cost and complexity of the fabrication. Another method of temperature compensation is to employ another intrinsic FP cavity adjacent to the pressure sensing cavity. In a recent study [12], a segment of single mode fiber was used as an intrinsic FP cavity for temperature measurement. The sensor was fabricated by using hydrofluoric acid (HF) etching, fusion splicing, cleaving, and polishing processes. The pressure sensitivity and temperature sensitivity were measured to be 3.97 nm/kPa with a 17 μm cavity and 6.8 nm/K with a 1000 μm cavity, respectively.

In this article, design, fabrication, and experimental study of a polymer/silica hybrid miniature dual-cavity FP sensor is presented for simultaneous pressure and temperature sensing. As illustrated in Fig. 1, the pressure sensing structure employs a UV molded cavity covered by a polymer/metal composite diaphragm. The low elastic modulus of the polymer/metal composite diaphragm renders the sensor a high pressure sensitivity even with a miniature size. The temperature sensing is achieved by using an intrinsic silica/polymer FP cavity that is adjacent to the pressure sensing cavity. By taking advantage of the large coefficient of thermal expansion (CTE) of the polymer, the sensor

Manuscript received November 5, 2013; revised January 8, 2014 and February 19, 2014; accepted February 19, 2014. Date of publication February 23, 2014; date of current version March 26, 2014. This work was supported by the U.S. National Science Foundation under Grant CMMI 1200420, National Institute of Standards and Technology under Grant 70NANB12H211, and TEDCO MII Phase I Grant.

H. Bae, D. Yun, and M. Yu are with the Department of Mechanical Engineering, University of Maryland, College Park, MD 20742 USA (e-mail: wwjd0691@gmail.com; davidyunjr@gmail.com; mmyu@umd.edu).

H. Liu is with the Department of Mechanical Engineering, University of Maryland, College Park, MD 20742 USA and also with the National Institute of Standards and Technology, Gaithersburg, MD 20899 USA (e-mail: liuhj@umd.edu).

D. A. Olson is with the National Institute of Standards and Technology, Gaithersburg, MD 200899 USA (e-mail: douglas.olson@nist.gov).

Color versions of one or more of the figures in this paper are available online at http://ieeexplore.ieee.org.

Digital Object Identifier 10.1109/JLT.2014.2308060

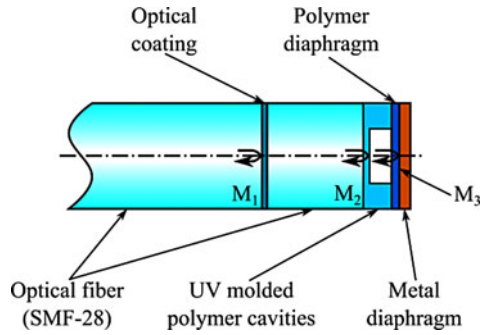

Fig. 1. Schematic of the hybrid temperature/pressure sensor.

can achieve a high temperature sensitivity with a short cavity length (the cavity length of the temperature sensing cavity: 284.8 μm) 71.5% smaller than that of the previously reported sensor made of silica material [12]. The sensor fabrication employs simple and safe procedures without using hazard acid (e.g., HF) and most processes can be performed in batch fabrication by adopting a wafer scale fabrication technique [20], [21]. To retrieve both temperature and pressure information from the dual cavities, a frequency domain demodulation scheme that is capable of acquiring multiple cavity lengths is developed.

II. Sensor Design and Fabrication

The dual-cavity FP pressure sensor is designed to have built-in temperature measurement and compensation capability, which consists of a spliced segment of single mode fiber, a UV molded cavity structure, and a polymer/metal composite diaphragm used as a pressure transducer. The schematic of the sensor is shown in Fig. 1. One of the cavities is an air cavity formed between the end surface of the UV-molded cavity (M_2) and a polymer/metal composite diaphragm (M_3), which is sensitive to both pressure and temperature change. The other cavity is an intrinsic silica/polymer hybrid FP cavity formed between an internal mirror (M_1) generated from multi-layer dielectric films evaporated on a fiber endface and the end surface of the UV-molded cavity (M_2). Since the silica/polymer cavity is only sensitive to temperature, it is used for temperature measurement.

To achieve high sensitivity pressure measurement, a large cavity diameter is desirable. However, the size of the cavity diameter is limited by that of the optical fiber. In this paper, the diameter of the air cavity (i.e., the size of the diaphragm) was designed to be 80 μm since an 80-μm diameter fiber is used as the mold in the fabrication process. By using a finite element model of the composite diaphragm, the thicknesses of the polymer layer and the metal layer in the composite diaphragm were chosen to be 0.5 and 0.2 μm, respectively. Note that these thicknesses were chosen to ensure high pressure sensitivity as well as to prevent the diaphragm from damage during the fabrication. The pressure sensitivity of the sensor was predicted to be 0.0145 μm/kPa at the room temperature. The air cavity length was designed to be 60 μm ensuring to have reasonably good number of fringes in the wavelength length range of the interrogation system.

On the other hand, in order to acquire a good temperature sensitivity, the silica/polymer cavity has to be properly designed. For a pure silica cavity, its temperature sensitivity can be expressed as

$$TS_{\text{silica}} = \left(\frac{\alpha_{n\_\text{silica}}}{n_{\text{silica}}} + CTE_{\text{silica}}\right) L_{\text{silica}} = (7.36\ \mu\varepsilon/^{\circ}\text{C})\, L_{\text{silica}}, \tag{1}$$

where α_{n_silica} is the thermo-optic coefficient, n_{silica} is the refractive index of the silica, CTE_{silica} is the CTE of silica, and L_{silica} is the length of the silica cavity. Since the thermo-optic coefficient ($1 \times 10^{-4}\ ^{\circ}\text{C}^{-1}$) and the CTE of silica (0.55 $\mu\varepsilon$/°C) are relatively low, in order to obtain a reasonable temperature sensitivity, the silica cavity length has to be relatively long [12]. However, a long cavity is not desirable in the design of a miniature fiber-optic sensor. To increase the temperature sensitivity of the sensor without increasing the length of the silica cavity, a thin polymer layer (OP-4–20632 UV curable polymer, Dymax)[1] with the refractive index of 1.553 (at 20°C and 589 nm wavelength) is added to the silica cavity, which has a CTE (54 $\mu\varepsilon$/°C) that is 98 times larger than that of silica and a thermo-optic coefficient of around $-3.6 \times 10^{-5}\ ^{\circ}\text{C}^{-1}$. Therefore, the overall temperature sensitivity of the silicon/polymer cavity can be rewritten as

$$\begin{aligned} TS_{\text{overall}} &= \left(\frac{\alpha_{n\_silica}}{n_{\text{silica}}} + CTE_{\text{silica}}\right) L_{\text{silica}} \\ &\quad + \left(\frac{\alpha_{n\_\text{polymer}}}{n_{\text{polymer}}} + CTE_{\text{polymer}}\right) L_{\text{polymer}} \\ &= (7.36\ \mu\varepsilon/^{\circ}\text{C}) L_{\text{silica}} + (30.32\ \mu\varepsilon/^{\circ}\text{C}) L_{\text{polymer}}, \end{aligned} \tag{2}$$

where $\alpha_{n\_\text{polymer}}$ is the thermo-optic coefficient of the UV curable polymer, n_{polymer} is the refractive index of the polymer, CTE_{polymer} is the CTE of the polymer material, L_{polymer} is the length of the polymer cavity.

In this paper, the silica cavity length and the added polymer thickness were chosen to be 250 and 35 μm, respectively, rendering a good temperature sensitivity of 0.0026 μm/°C. Because of the small refractive index difference between the UV curable polymer and the silica, the reflection at the silica/polymer interface is negligible. In addition, the relatively long cavity length of the silica ensures that there are enough number fringes in the interference spectrum and helps separate the optical frequency of the temperature sensing cavity from that of the pressure sensing cavity for easy signal processing.

In order to obtain accurate measurements from the two optical cavities, the two cavities should be carefully designed to ensure a good visibility of the multi-frequency interference fringes. Reflection from the internal mirror (M_1) can be tuned by changing

[1]Certain commercial equipment, instruments, or materials are identified in this paper to foster understanding. Such identification does not imply endorsement by NIST nor does it imply that the equipment or materials are necessarily the best available for the purpose.

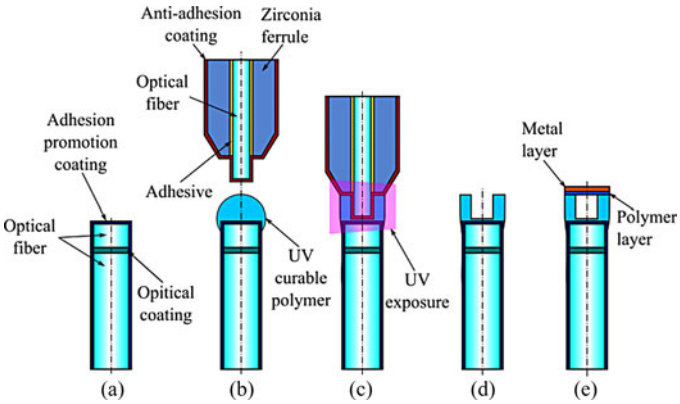

Fig. 2. Fabrication process of the hybrid UV-molded temperature/pressure sensor.

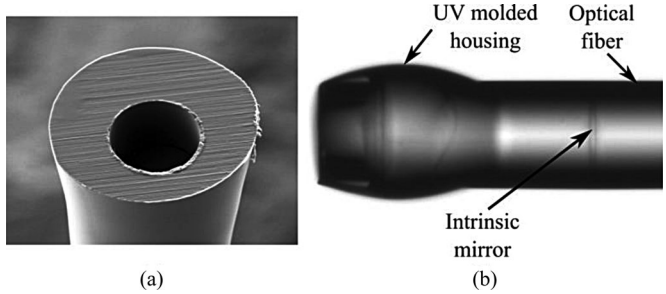

Fig. 3. (a) Close-up SEM of a molded cavity and (b) microscopic image of the fabricated sensor before depositing a metal layer.

the number of alternating layers of TiO_2 and SiO_2. Furthermore, the parameters used for splicing should also be well chosen to obtain proper reflectivity of M_1 for a good spectrum visibility. In this paper, the reflectivity of M_1 was chosen to be 4%, the same as that of M_2 that is due to the Fresnel reflection between polymer and air.

The sensor fabrication is composed of three steps. The first step is to splice a segment of single mode fiber that is used as part of the silica/polymer cavity for temperature measurement. The second step is to perform cavity molding. Finally, in the third step, a metal-polymer composite diaphragm is covered over the molded cavity. The detailed fabrication process is shown in Fig. 2. After a batch of single mode fibers (Corning, SMF-28e) were prepared by cleaving and cleaning, the fiber endfaces are coated with five alternating layers of TiO_2 and SiO_2, each with a quarter wavelength thickness (at $\lambda = 850$ nm), by using electron beam evaporation. Another optical fiber was then spliced to the fiber with the optical coatings with empirically determined conditions to obtain the designed reflectivity ($\approx 4\%$). The splicing was performed with a commercial fusion splicer (Hamamatsu, Type-36) with 2 arc count and 0.5 s arc duration in order to get desired reflectivity from the fabricated internal mirror [22]–[24]. The fiber was then cleaved under a microscope to be around 250 μm away from the spliced location [see Fig. 2(a)]. Then, the prepared fiber is preliminarily aligned to a mold, constructed by using an 80-μm single mode optical fiber and a zirconia ferrule, under two optical microscopes with CCD cameras positioned with a 90° angle separation under the assistance of two five-axis manual stages. A small drop of a UV curable polymer is deposited at the end of the prepared fiber by retracting the fiber approximately by 500 μm [see Fig. 2(b)]. After this, the fiber with the deposited polymer is carefully moved toward the mold until the fiber endface touches the mold, followed by retracting with a precision stage to obtain a desired polymer thin film between the fiber mode and the endface of the sensing fiber [see Fig. 2(c)]. By using the optical fiber based mold, an accurate core-to-core alignment is enabled by monitoring the coupling intensity between the fiber and mold. A detailed description is provided in the author's previous work [16]. Further, post-baking is performed as the last step of the polymer housing fabrication at 150 °C for 5 h to achieve good thermal and mechanical stability of the UV-cured polymer housing. Finally, a polymer-metal composite layer is deposited on the housing structure to form a suspended diaphragm. The diaphragm fabrication process is as follows. A drop of UV curable polymer (OP-4–20641, Dymax) is dispensed onto the distilled water contained in a petri dish with 100 mm diameter. The dispensed polymer spreads out to form a uniform and thin layer. By controlling the volume of the dispensed polymer, the thickness of the thin polymer layer can be well controlled. The floating polymer layer is then half-cured on the water surface with a flood UV light source (Model 22-UV, Optical Engineering, INC) for 7 min, followed by lifting up the diaphragm from water and covering it on a batch of the molded cavities. Detailed polymer diaphragm covering process is provided in our previous work [25]. Additionally, a post UV-curing with a spot UV light source (Blue Wave 50AS, Dymax) for 100 s and thermal curing at 150 °C for 3 h is performed to enhance the stability of the UV-curable polymer. This batch fabrication process ensures a good device-to-device uniformity and low fabrication cost. Finally, the polymer diaphragm is deposited with a titanium and silver layer using a direct current magnetron sputtering machine. A close-up scanning electron micrograph (SEM) of the molded cavity and a microscopic image of the fabricated sensor before covering a metal layer are shown in Fig. 3.

III. Optical Interrogation and Signal Processing

In the experiment, the fabricated sensor was connected to a broadband optical interrogation system, which is consisted of a 2×2 coupler (Gould Fiber Optics), a broadband spectrometer (USB4000, Ocean Optics) with 0.4 nm wavelength resolution, and a broadband light source (HL-2000, Ocean Optics). The broadband spectrometer has a large wavelength bandwidth from 700 to 1000 nm, which ensures a good optical frequency resolution in the data processing using fast Fourier transform (FFT). The experimental arrangement for pressure and temperature calibration is illustrated in Fig. 4. The spectrum of the multi-cavity FP sensor has a combination of distinctive optical frequencies, which are defined by the air cavity, silica/polymer cavity, and the combination of those two cavities. The total intensity of

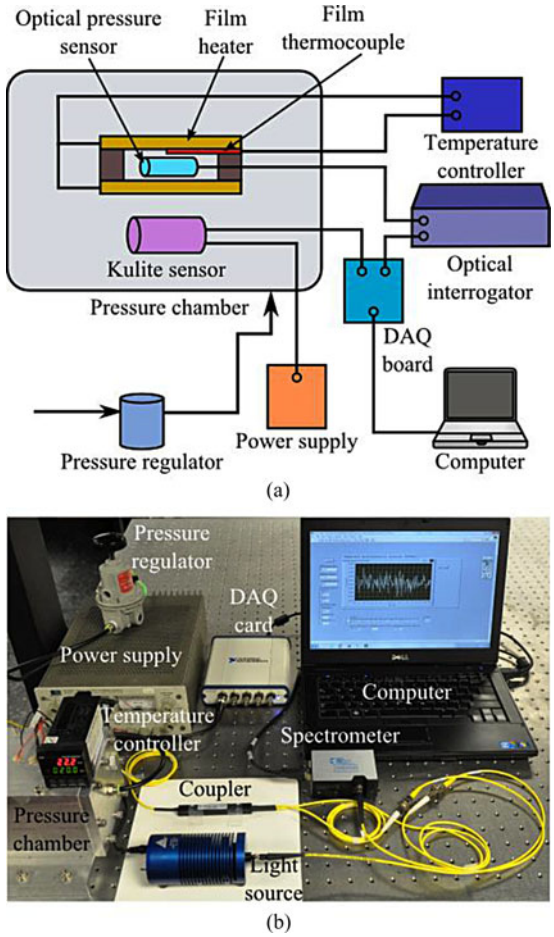

Fig. 4. Experiment arrangement for pressure measurement: (a) schematic and (b) photograph of the setup.

interference can be written as [26]

$$
\begin{aligned}
I(\lambda) &= \left| \begin{array}{l} A_1 - A_2 \exp\left(-\frac{j4\pi(n_{\text{silica}}L_{\text{silica}}+n_{\text{polymer}}L_{\text{polymer}})}{\lambda}\right) \\ +A_3 \exp\left(-\frac{j4\pi(n_{\text{silica}}L_{\text{silica}}+n_{\text{polymer}}L_{\text{polymer}}+L_{\text{air}})}{\lambda}\right) \end{array} \right|^2 \\
&= A_1^2 + A_2^2 + A_3^2 - 2A_1A_2 \\
&\quad \cos\left(\frac{4\pi(n_{\text{silica}}L_{\text{silica}} + n_{\text{polymer}}L_{\text{polymer}})}{\lambda}\right) \\
&\quad - 2A_2A_3 \cos\left(\frac{4\pi(L_{\text{air}})}{\lambda}\right) \\
&\quad + 2A_3A_1 \\
&\quad \cos\left(\frac{4\pi(n_{\text{silica}}L_{\text{silica}} + n_{\text{polymer}}L_{\text{polymer}} + L_{\text{air}})}{\lambda}\right),
\end{aligned} \tag{3}
$$

where A_1, A_2, and A_3 are the amplitudes of the reflected electric fields that are related to reflectivity of the internal mirror, the air cavity bottom surface, and the composite diaphragm, respectively, L_{air} is the length of the air cavity, and λ is the free-space wavelength.

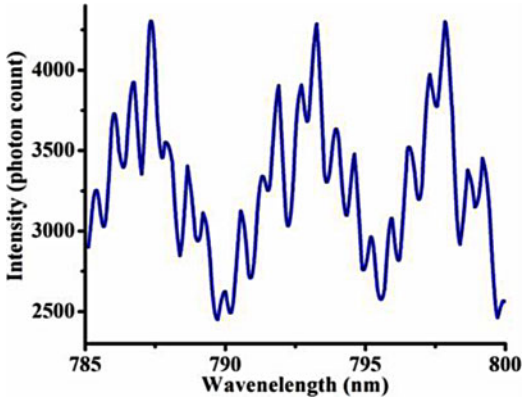

Fig. 5. Interference spectrum of the fabricated sensor obtained with the broadband interrogation system.

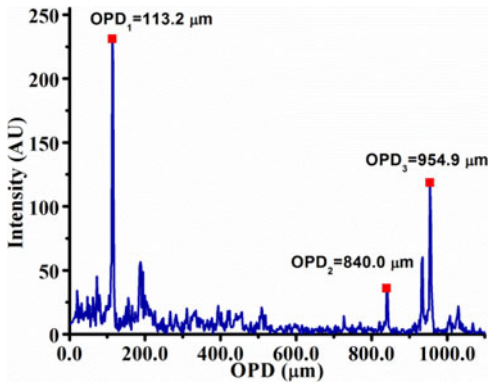

Fig. 6. FFT result from the wavenumber spectrum of the sensor.

A representative interference spectrum obtained from the sensor by using the broadband optical interrogation system is shown in Fig. 5. The low frequency waveform in the spectrum corresponds to the air cavity and the high frequency modulations are due to the silica/polymer cavity and the combination of the two cavities.

In order to retrieve the two cavities independently, optical frequency domain signal processing was adopted. The acquired wavelength spectrum was first converted to the wavenumber domain. Since the obtained wavenumber spectrum is not evenly spaced, cubic spline interpolation and resampling were performed. An FFT of the resampled spectrum was carried out and the optical path differences (OPDs) were determined based on the FFT results. The relationship between the measured OPD and the optical cavity length can be described as

$$\text{OPD} = 2nL = f, \tag{4}$$

where L is the optical cavity length, and n is the refractive index of the FP cavity. Fig. 6 shows the FFT result of a sensor wavenumber spectrum. The three peaks shown in the figure correspond to the air cavity, the silica/polymer cavity, and the combination of the two cavities. The cavity lengths obtained from the FFT result are 56.62 and 284.83 μm, respectively, for the air cavity and the silica/polymer cavity. However, the FFT results only provide limited resolution in the cavity lengths due to the limited wavelength range (700 to 1000 nm) of the

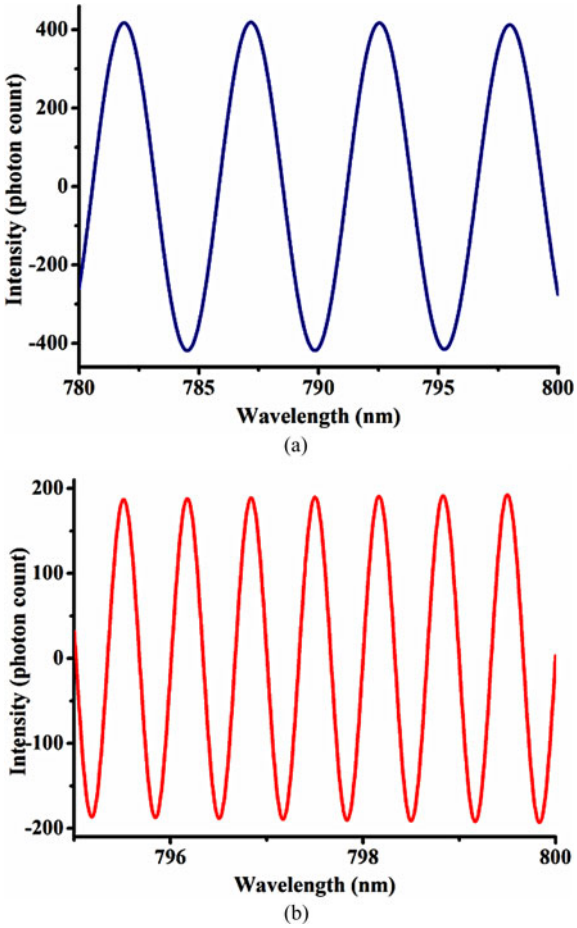

Fig 7. Filtered wavelength spectrum for (a) the air cavity and (b) the combined cavity of air and silica/polymer. The dc component of the intensity was removed.

spectrometer [27]. Increasing the wavelength range is costly and can result in a reduced sampling rate of the detection system. In order to achieve a better accuracy of the cavity lengths without compromising the sampling rate, a method that makes use of curve fitting of the filtered spectrum has been previously reported [28]. However, this method is computationally costly since it needs to utilize the entire spectrum to obtain a fitted curve and requires iterative calculations.

In this paper, a novel signal processing scheme is developed, which makes use of selective curve fitting to the filter spectrum and combines with the one peak tracing method [29]. In this method, the measured optical frequencies from the FFT result are used as the center frequencies of band-pass Butterworth filters to extract the single frequency wavelength spectrum at the frequency of interest. Fig. 7 shows the filtered wavelength spectra by using two different band-pass filters whose center frequencies are corresponding to the two peaks (OPD_1 and OPD_3) in the FFT result shown in Fig. 6. After obtaining the spectrum with a single frequency matching to each cavity length, curve fitting is performed only at the peak region of the spectrum. The one peak tracing method is then used to retrieve the value of the cavity length.

By using this method, the cavity length can be determined with a high resolution (0.2 nm with USB4000 spectrometer) due to the nature of the one peak tracking method [29]. The resolution was determined by measuring the root-mean-square error of the cavity length measurement. This resolution is much higher than that obtained directly from the FFT method (845.1 nm with the same spectrometer). The resolution of the FFT method was determine by minimum theoretical step size of the cavity length measurement (i.e., the maximum achievable resolution). The resolution of the FFT method is limited by the wavelength range of the spectrometer (700–1000 nm) used in the measurement. Furthermore, the calculation time can be reduced significantly (around 19 times faster according to the simulations) compared to the band-pass filtering and spectrum curve fitting method [28] because in this paper the curve fitting is only performed at the vicinity of each peak.

A parametric study was carried out to compare the performance of the demodulation scheme developed in this paper with the previously reported method in terms of calculation time and linearity of the cavity measurements. In the simulations, a sensor with two cavities with initial cavity lengths of 60 and 300 μm were used. Both of the two cavity lengths were varied by 0.05 μm with a step of 0.001 μm (i.e., 60.000 μm cavity was increased to 60.050 μm and 300.000 μm cavity to 300.050 μm with 0.001 μm step). Random noise was introduced to the interference signals in the simulation to simulate inherent noise of a spectrometer and a light source. The cavity length changes were retrieved from the simulated spectrum by using the full spectrum curve fitting method [28] and the method developed in this paper. R^2 values of the determined cavity length as a function of the true cavity length were obtained and plotted as a function of signal-to-noise ratio (SNR) for the two different methods, shown in Fig. 8. It can be seen that both methods were able to retrieve the cavity length change with a good linear performance when the SNR is high. However, when the SNR is low, the method developed in this paper shows a better resilience to noise over the previous method. Moreover, it was found during the simulations that the method developed in this paper was about 19 times faster with a calculation speed of 0.46 s per data point, while for the previously reported method, the calculation speed was 8.71 s per data point.

IV. Sensor Calibration

The calibration of the sensor for pressure measurement was performed in a pressure chamber with a reference pressure sensor, as shown in Fig. 4. A conventional pressure sensor (LL-080–35A, Kulite Semiconductor) with a pressure uncertainty of 1% or 3.35 kPa in the pressure range of 0 to 344.74 kPa was used as the reference. The internal chamber pressure was controlled by using a pressure regulator (Pressure Regulator Type 70, Marsh Bellofram), which has a gauge mode pressure range of 0 to 206.84 kPa. Temperature control was achieved by using a temperature controller (Omega Engineering Inc., CN77333), a polyimide-insulated flexible thermocouple (Omega Engineering Inc., CO1-K) with an uncertainty of 1.5% or 4.0 °C in the temperature range of 0 to 260 °C, and two polyimide-insulated flexible heaters (Omega Engineering Inc., KH 103/10). The heaters were place above and below the sensor to control the temperature

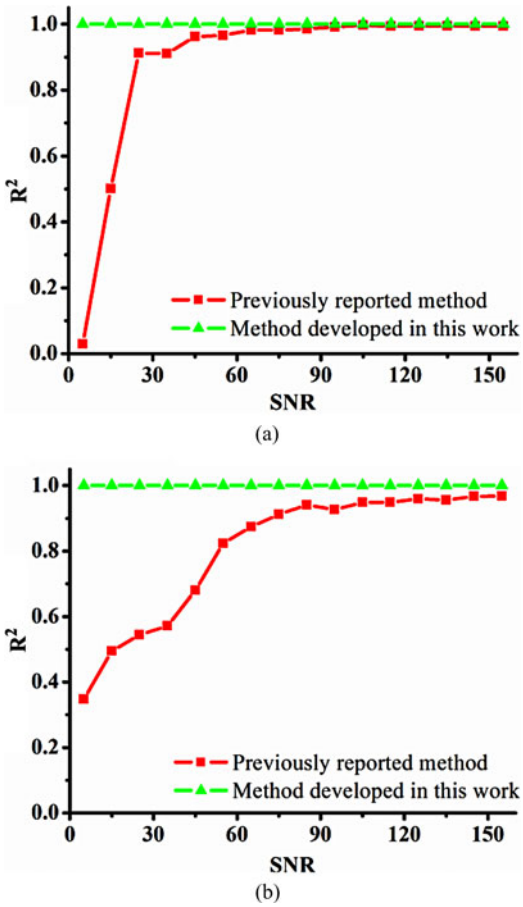

Fig. 8. Comparison of R^2 values as a function of SNR by using two different demodulation schemes (spectrum curve fitting and one peak tracking of the filtered spectrum) for cavity lengths: (a) 60 μm and (b) 300 μm. SNR was calculated as the signal power divided by the noise power.

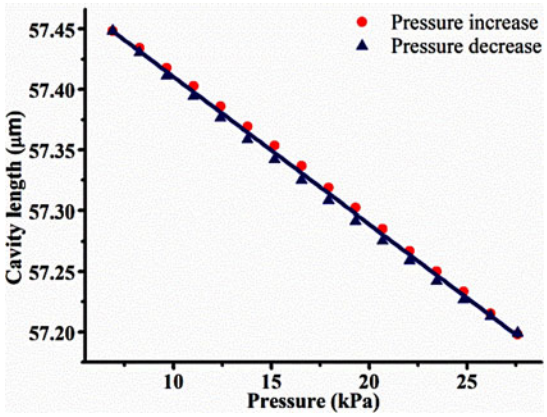

Fig. 9. Pressure calibration curves of the sensor at 26.0 °C.

locally, while minimizing the heating time and the temperature effect on the reference pressure sensor.

In the experiments, at a room temperature of 26 °C, the pressure in the chamber was first increased and then decreased with a step of 1.38 kPa within a range of 6.89 to 27.58 kPa. The calibration result of the sensor is shown in Fig. 9. It can be seen that the sensor exhibits a good linearity ($R^2 = 0.9993$) over the entire tested pressure range. Based on the linear regression analysis of the measured data, the pressure sensitivity was calculated to be 0.0122 μm/kPa with an uncertainty of 0.0002 μm/kPa (1.6%). This result is slightly smaller than the predicted value obtained from the numerical simulations (0.0145 μm/kPa). Residual stresses generated during the polymerization and metallization process of the diaphragm are the possible reasons for the lower measured sensitivity. Furthermore, the sputtering process induced a curvature in the diaphragm, which further reduces the pressure sensitivity. To obtain the pressure resolution, the cavity length was first measured for a fixed pressure level at the room temperature and the root mean square (RMS) error of the cavity length was calculated. Note that the RMS error represents the noise floor of the cavity length measurement, which is determined by the overall noise of the measurement system including the sensor and the optical interrogation system. Therefore, the pressure resolution can be obtained by using the RMS error divided by the measured pressure sensitivity of the sensor. Based on this method, the pressure resolution of the FP pressure sensor was determined to be 0.021 kPa. The sources of the noise in the pressure measurement include the mechanical–thermal noise of the pressure sensor and the noise of the optical interrogation system. Based on the Nyquist relation [30], the sensor mechanical–thermal noise was calculated to be 2.5% of the overall noise floor. Therefore, the noise of the optical interrogation system is the dominant noise source, which includes the shot-noise, the thermal-noise, the amplifier noise of the spectrometer, and the relative intensity noise of the light source [31]. In addition, the hysteresis error and the pressure uncertainty of the sensor were obtained to be 0.476 (2.3%) and 0.126 kPa (0.6%), respectively. The small zero drift and nonlinearity of the calibration curves are believed to be mainly due to temperature variations of the environment (~0.2 °C) since the temperature was not controlled to be constant during the pressure calibrations.

To evaluate the temperature effect, the pressure sensitivities for both the air cavity and the silica/polymer cavity were obtained at different temperatures (e.g., 26, 34, 42, and 50 °C) by using the experimental setup shown in Fig. 4. The pressure calibration result of the air cavity is shown in Fig. 10(a). In all four cases, the measurement results show good linearity ($R^2 > 0.9994$) over the measured pressure range. However, it can be seen that pressure sensitivities have temperature dependency. The deviation of the sensitivity value is believed to be due to the Young's modulus change of the polymer layer in the polymer/metal composite diaphragm and the UV molded cavity due to the temperature. In Fig. 10(b), the pressure sensitivities of the silica/polymer cavity at the four different temperatures are plotted. It can be seen that due to the high elastic modulus of silica (71.7 GPa), the cavity length change of the temperature sensing cavity with respect to pressure is negligible in the pressure range of 6.89 to 27.58 kPa for all four temperatures. The slight fluctuations of the cavity length are believed to be mainly due to temperature fluctuations from the temperature controller.

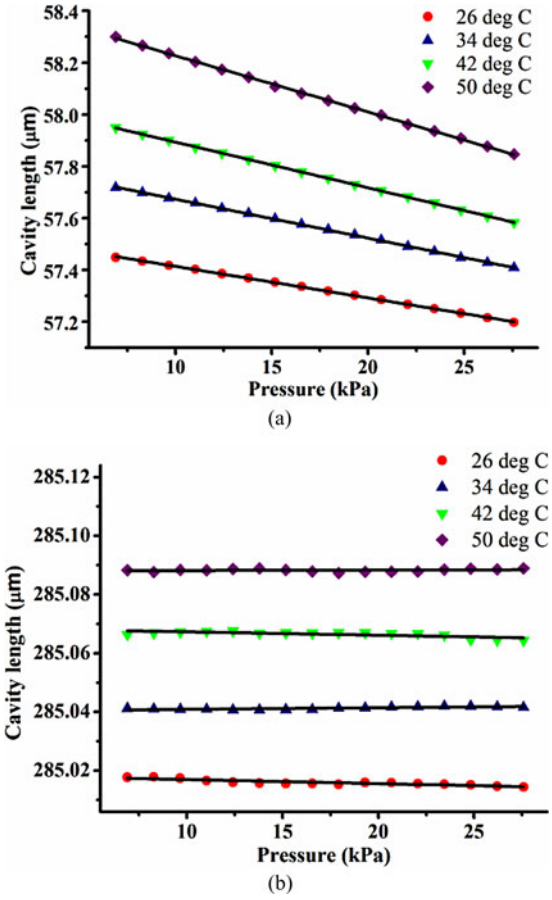

Fig. 10. Pressure calibration curves: (a) air cavity and (b) silica/polymer cavity at four different temperatures (26.0, 34.0, 42.0, and 50.0 °C).

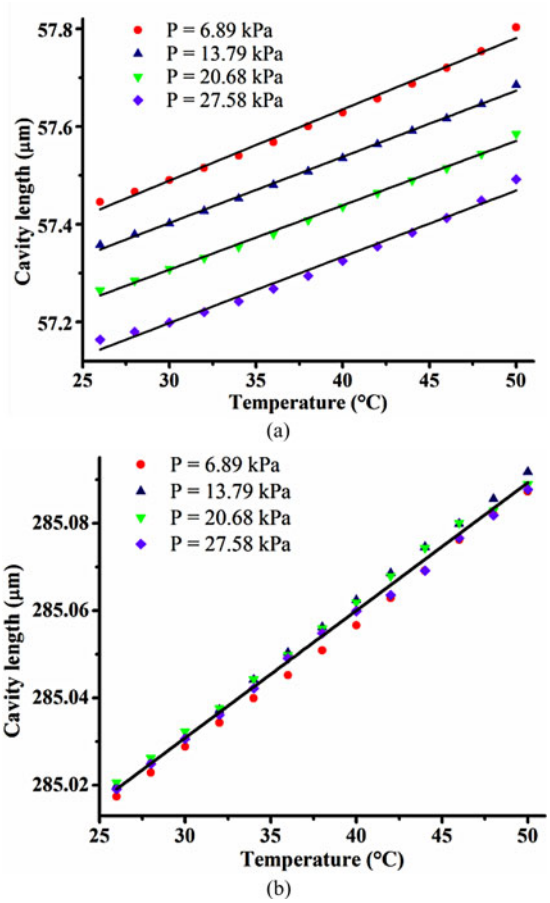

Fig. 11. Temperature calibration curves: (a) air cavity and (b) silica/polymer cavity at four different pressure levels of 6.89, 13.79, 20.68, and 27.58 kPa.

V. Temperature Sensitivity and Temperature Compensation

As discussed previously, the silica/polymer FP cavity in the fabricated sensor can be used as a temperature sensor due to its linear response to temperature change and low pressure sensitivity. In addition, the temperature reading from the silica/polymer cavity can be used to compensate for the relatively large temperature drift of the pressure sensing cavity. To evaluate the temperature sensing performance of the silica/polymer cavity and the temperature compensation capability of the sensor, temperature calibration of the two cavities was performed in the pressure chamber with a temperature controller, as shown in Fig. 4.

First, the temperature sensitivity of the air cavity was evaluated. In the experiment, the temperature sensitivity of the cavity was measured by monitoring the cavity length change of the air FP cavity with respect to the temperature change. To measure the temperature sensitivity, the sensor was heated from 26 to 50 °C with an increment of 2 °C under four different pressure levels 6.89, 13.79, 20.68, and 27.58 kPa. The cavity lengths were recorded as a function of temperature at each pressure level. The obtained temperature calibration results of the air FP cavity are shown in Fig. 11(a). According to the result, a linear relationship between the air cavity length and temperature can be observed with a good linearity ($R^2 > 0.9881$) and a sensitivity of 0.0137 μm/°C with an uncertainty of 0.0003 μm/°C (2.2%).

Next, the temperature sensitivity and temperature resolution of the silica/polymer FP cavity were investigated. By using the same experimental arrangement and method, the temperature calibration results for the silica/polymer cavity at several different pressures were obtained, as shown in Fig. 11(b). The calibration results exhibit a good linearity ($R^2 > 0.9984$) and the pressure sensitivity of the silica/polymer cavity is found to be negligible. The temperature sensitivity and resolution of the silica/polymer cavity of the FP pressure sensor were obtained as 0.0029 μm/°C with an uncertainty of 0.0001 μm/°C (3.4%) and 0.10 °C, respectively. The uncertainty of the temperature measurement was 0.03 °C (0.14%). By using the hybrid silica/polymer cavity, a high temperature sensitivity as well as a high resolution can be achieved with a smaller form factor compared to the sensor made of pure silica.

In order to compensate for the temperature effect of the pressure sensing cavity, the temperature readings from the silica cavity are used along with the temperature sensitivity of the air cavity. Based on Fig. 11(b), the relationship between the silica/polymer cavity length and the temperature can be obtained

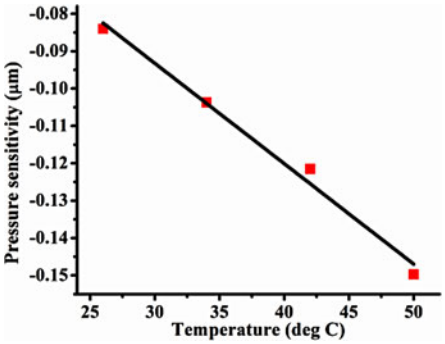

Fig. 12. Pressure sensitivity of the air cavity as a function of temperature.

as

$$T = (L_{\text{silica/polymer}} - L^0_{\text{silica/polymer}})/TS_{\text{silica/polymer}} + T^0, \quad (5)$$

where T is the measured temperature, T^0 is the initial temperature, $L_{\text{polymer/silica}}$ is the cavity length of the silica/polymer cavity, $L^0_{\text{silica/polymer}}$ is the initial cavity length of the silica/polymer cavity, and $TS_{\text{silica/polymer}}$ is the temperature sensitivity of the silica/polymer cavity.

It is noted that the pressure sensitivity of the sensor varies from 0.0122 to 0.0218 μm/kPa in the temperature range of 26 to 50 °C. This large sensitivity change is believed to be due to softening of the polymer layer in the polymer/metal composite diaphragm. Also, this change was found to be reversible. The pressure sensitivity as a function of the temperature is shown in Fig. 12, which was found to be a linear function. Based on this figure, the pressure sensitivity can be obtained at any temperature as

$$PS_{\text{air cavity}}(T) = (0.00269T + 0.0018)\ \mu\text{m/kPa}, \quad (6)$$

where $\text{PS}_{\text{air cavity}}$ is the pressure sensitivity of the air cavity and T is the temperature. The measured pressure sensitivity can then be used to compensate the temperature effect. As shown in Figs. 10 and 11, the lengths of the air and the silica/polymer cavities change linearly with respect to both pressure and temperature. Therefore, the temperature-compensated pressure can be expressed as the following:

$$P = \frac{(L_{\text{air}} - TS_{\text{air cavity}}(T - T^0) - L^0_{\text{air}})}{-PS_{\text{air cavity}}(T)} + P^0 \quad (7)$$

where P is the measured pressure, L_{air} is the cavity length of the air cavity, L^0_{air} is the initial cavity length of the air cavity, $TS_{\text{air cavity}}$ is the temperature sensitivity of the air cavity, and P^0 is the initial pressure. Based on (5) and (7), the temperature and pressure values can be retrieved simultaneously from the measurement results of the two FP cavity length changes.

VI. Concluding Remarks

In this article, a hybrid dual Fabry–Perot cavity fiber optic pressure and temperature sensor is presented. The sensor, which is made at the end of a single mode fiber, is composed of an air cavity for pressure sensing and a polymer/silica hybrid cavity for temperature sensing. The dual cavity design renders the sensor the capability of temperature compensation and simultaneous pressure and temperature measurements. The fabrication of the extrinsic air cavity was performed by using a unique UV molding process with an optical fiber based mold. The intrinsic silica/polymer cavity formed between several layers of dielectric optical coating and the bottom surface of the UV molded cavity enables a high temperature sensitivity of the sensor with a small cavity length, owing to the large thermal expansion of the polymer material. Due to the relatively low stiffness of the polymer/metal composite diaphragm, a sensor with a miniature size but having a high sensitivity can be obtained. Experimental studies have shown that the sensor has good linearity for pressure measurement in the designed pressure range. Effective temperature measurement by using the embedded intrinsic silica/polymer cavity has also been demonstrated. Furthermore, a novel signal processing method has been developed for demodulation of multiple cavity lengths for multiplexed FP sensors or a FP sensor with multiple cavities. Compared with the previous methods, this method renders much shorter calculation time, higher resolution, and better resilience to noise.

References

[1] Y. Rao and D. A. Jackson, "Recent progress in fibre optic low-coherence interferometry," *Meas. Sci. Technol.*, vol. 7, pp. 981–999, 1996.
[2] W. N. MacPherson, J. M. Kilpatrick, J. S. Barton, and J. D. C. Jones, "Miniature fiber optic pressure sensor for turbomachinery applications," *Rev. Sci. Instrum.*, vol. 70, no. 3, pp. 1868–1874, 1999.
[3] D. C. Abeysinghe, S. Dasgupta, H. E. Jackson, and J. T. Boyd, "Novel MEMS pressure and temperature sensors fabricated on optical fibers," *J. Micromech. Microeng.*, vol. 229, pp. 229–235, 2002.
[4] M. J. Gander, W. N. MacPherson, J. S. Barton, R. L. Reuben, J. D. C. Jones, R. Stevens, K. S. Chana, S. J. Anderson, and T. V. Jones, "Embedded micromachined fiber-optic Fabry–Perot pressure sensors in aerodynamics applications," *IEEE Sens. J.*, vol. 3, no. 1, pp. 102–107, Feb. 2003.
[5] D. Donlagic and E. Cibula, "All-fiber high-sensitivity pressure sensor with SiO2 diaphragm," *Opt. Lett.*, vol. 30, no. 16, pp. 2071–2073, 2005.
[6] J. Xu, X. Wang, K. L. Cooper, and A. Wang, "Miniature all-silica fiber optic pressure and acoustic sensors," *Opt. Lett.*, vol. 30, no. 24, pp. 3269–3271, Nov. 2005.
[7] X. Wang, J. Xu, Y. Zhu, K. L. Cooper, and A. Wang, "All-fused-silica miniature optical fiber tip pressure sensor," *Opt. Lett.*, vol. 31, no. 7, pp. 885–887, Apr. 2006.
[8] W. Wang, N. Wu, Y. Tian, C. Niezrecki, and X. Wang, "Miniature all-silica optical fiber pressure sensor with an ultrathin uniform diaphragm," *Opt. Exp.*, vol. 18, no. 9, pp. 9006–9014, Apr. 2010.
[9] F. Guo, T. Fink, M. Han, L. Koester, J. Turner, and J. Huang, "Fabry–Perot interferometric fiber-tip sensor based on a thin silver diaphragm," *Opt. Lett.*, vol. 37, no. 9, pp. 1505–1507, 2012.
[10] F. Interferometer, W. Wang, Q. Yu, F. Li, X. Zhou, and X. Jiang, "Temperature-insensitive pressure sensor based on all-fused-silica extrinsic Fabry–Pérot optical," *IEEE Sens. J.*, vol. 12, no. 7, pp. 2425–2429, Jul. 2012.
[11] J. Ma, W. Jin, H. L. Ho, and J. Y. Dai, "High-sensitivity fiber-tip pressure sensor with graphene diaphragm," *Opt. Lett.*, vol. 37, no. 13, pp. 2493–2495, Jul. 2012.
[12] S. Pevec and D. Donlagic, "Miniature all-fiber Fabry–Perot sensor for simultaneous measurement of pressure and temperature," *Appl. Opt.*, vol. 51, no. 19, pp. 4536–4541, 2012.
[13] Y. Wang, D. N. Wang, C. Wang, and T. Hu, "Compressible fiber optic micro-Fabry–Pérot cavity with ultra-high pressure sensitivity," *Opt. Exp.*, vol. 21, no. 12, p. 14084, Jun. 2013.
[14] G. Hill, R. Melamud, A. Davenport, F. Declercq, I. Chan, P. Hartwell, and B. Pruitt, "SU-8 MEMS Fabry–Perot pressure sensor," *Sens. Actuators, A*, vol. 138, no. 1, pp. 52–62, Jul. 2007.
[15] H. Bae, L. Dunlap, J. Wong, and M. Yu, "Miniature temperature compensated Fabry–Perot pressure sensors created with self-aligned polymer

photolithography process," *IEEE Sens. J.*, vol. 12, no. 5, pp. 1566–1573, May 2012.
[16] H. Bae and M. Yu, "Miniature fabry-perot pressure sensor created by using UV-molding process with an optical fiber based mold," *Opt. Exp.*, vol. 20, no. 13, p. 14573, Jun. 2012.
[17] Q. Wang, L. Zhang, C. Sun, and Q. Yu, "Multiplexed fiber-optic pressure and temperature sensor system for down-hole measurement," *IEEE Sens. J.*, vol. 8, no. 11, pp. 1879–1883, Nov. 2008.
[18] K. Bremer, E. Lewis, G. Leen, B. Moss, S. Lochmann, and I. Mueller, "Temperature compensated miniature all-glass fibre optic pressure sensor," in *Proc. IEEE Sens.*, 2011, pp. 105–108.
[19] H. Bae and M. Yu, "Investigation of miniature fiber optic surface-mountable fabry-perot pressure sensor built on 45° angled fiber," in *Proc. SPIE 7981, Sens. Smart Struc. Technol. Civil, Mech., Aerosp. Syst.*, 2011, pp. 79812X-1–79812X-7.
[20] P. Dannberg, L. Erdmann, A. Krehl, C. Wachter, and A. Brauer, "Integration of optical interconnects and optoelectronic elements on wafer-scale," *Mater. Sci. Semicond. Process.*, vol. 3, pp. 437–441, 2000.
[21] J. Duparré, P. Dannberg, P. Schreiber, A. Bräuer, and A. Tünnermann, "Artificial apposition compound eye fabricated by micro-optics technology," *Appl. Opt.*, vol. 43, no. 22, pp. 4303–4310, 2004.
[22] M. N. Inci, S. R. Kldd, J. S. Barton, and J. D. C. Jones, "Fabrication of single-mode fibre optic Fabry–Perot interferometers using fusion spliced titanium dioxide optical coatings," *Meas. Sci. Technol.*, vol. 3, pp. 678–684, 1992.
[23] H. Y. Choi, K. S. Park, S. J. Park, U.-C. Paek, B. H. Lee, and E. S. Choi, "Miniature fiber-optic high temperature sensor based on a hybrid structured Fabry–Perot interferometer," *Opt. Lett.*, vol. 33, no. 21, pp. 2455–2457, Nov. 2008.
[24] C. E. Lee, W. N. Gibler, R. A. Atkins, and H. F. Taylor, "In-line fiber Fabry–Perot interferometer with high-reflectance internal mirrors," *J. Light. Technol.*, vol. 10, no. 10, pp. 1376–1379, 1992.
[25] S. Nesson, M. Yu, X. Zhang, and A. H. Hsieh, "Miniature fiber optic pressure sensor with composite polymer-metal diaphragm for intradiscal pressure measurements," *J. Biomed. Opt.*, vol. 13, no. 4, p. 044040, 2008.
[26] Y. Zhu and A. Wang, "Miniature fiber-optic pressure sensor," *IEEE Photon. Technol. Lett.*, vol. 17, no. 2, pp. 447–449, Feb. 2005.
[27] Y. Jiang, "Fourier transform white-light interferometry for the measurement of fiber-optic extrinsic Fabry–Pérot interferometric sensors," *IEEE Photon. Technol. Lett.*, vol. 20, no. 2, pp. 75–77, Jan. 2008.
[28] F. Shen and A. Wang, "Frequency-estimation-based signal-processing algorithm for white-light optical fiber Fabry–Perot interferometers," *Appl. Opt.*, vol. 44, no. 25, pp. 5206–5214, Sep. 2005.
[29] B. Qi, G. R. Pickrell, J. C. Xu, P. Zhang, Y. H. Duan, W. Peng, Z. Y. Huang, W. Huo, H. Xiao, R. G. May, and A. Wang, "Novel data processing techniques for dispersive white light interferometer," *Opt. Eng.*, vol. 42, no. 11, pp. 3165–3171, 2003.
[30] T. B. Gabrielson, "Mechanical-thermal noise in micromachined acoustic and vibration sensors," *IEEE Trans. Electron. Dev.*, vol. 40, no. 5, pp. 903–909, May 1993.
[31] G. P. Agrawal, "Optical Receivers," in *Fiber-Optic Communication Systems*, 3rd ed. New York, NY, USA: Wiley, 2002, pp. 155–159.

Hyungdae Bae received the B.S. and M.S. degrees in mechanical engineering from Yonsei University, Seoul, Korea, in 2004 and 2006, respectively, and the Ph.D. degree in mechanical engineering from the University of Maryland, College Park, MD, USA, in 2013. He is currently a Research Assistant with the Department of Mechanical Engineering, the University of Maryland. His current research interests include miniature fiber optic pressure/temperature sensor, temperature compensation of fiber optic sensors, and micro/nano fabrication of optical element based on polymer processing. Dr. Bae was a nominee of A. James Clark School of Engineering Fellowship from 2008 to 2011 from the University of Maryland and has a U.S. patent on ultra-miniature fiber-optic pressure sensor system and method of fabrication.

David Yun is currently a Junior working toward the B.S. degree in mechanical engineering and the B.A. degree in piano performance at the University of Maryland, College Park, MD, USA. In 2012, he was a Lab Intern for the Mechanical Engineering Department, the University of Maryland, assisting research of fiber optic pressure/temperature sensor. Mr. Yun is a recipient of the President's Scholarship from the University of Maryland and is part of the Honor's College there.

Haijun Liu received the B.S. degree in mechanical engineering and the M.S. degree in materials science from Tsinghua University, Beijing, China, in 2002 and 2005, respectively, and the Ph.D. degree in mechanical engineering from the University of Maryland, College Park, MD, USA, in 2012. He is currently a Research Associate with the Department of Mechanical Engineering, University of Maryland and a Guest Researcher with the Sensor Science Division of the National Institute of Standards and Technology, Gaithersburg, MD, USA. His current research interests include bio-inspired acoustic sensors, dynamic pressure measurement in shock wave, acoustic metamaterial, and micro/nano systems in general. He was a future Faculty Fellow from the A. James Clark School of Engineering of the University of Maryland in 2009. He has a U.S. patent on Biology-inspired miniature system and method for sensing and localizing acoustic signals.

Douglas A. Olson received the Ph.D. degree from the Massachusetts Institute of Technology, Cambridge, MA, USA, in 1987. He currently directs the high pressure metrology project in the Sensor Science Division of the National Institute of Standards and Technology (NIST). This project is responsible for traceability and dissemination of the SI unit of pressure in the United States of America from 10 kPa to 300 MPa. He has published widely in the field of pressure metrology and represents NIST on international metrology committees. His current research interests include miniature fiber-optic pressure sensors, optical methods for static and dynamic pressure measurement, and the automation of pressure calibration. Dr. Olson is the recipient of the 2013 Judson C. French award at NIST.

Miao Yu received the Ph.D. degree from the University of Maryland, College Park, MD, USA, in 2002. She is currently an Associate Professor of the Department of Mechanical Engineering, the University of Maryland with an expanded range of research interests encompassing bio-inspired systems, sensors and actuators, light and matter interactions, plasmonics and metamaterials, microsystems and nanosystems, and smart materials and structures. Dr. Yu awards and honors include the receipt of the 2006 Ralph E. Powe Junior Faculty Enhancement Award (2006), the NSF CAREER Award (2007), and the AFOSR Young Investigator Award (2008).